Finite Element Analysis of the ACL-deficient Knee

David Jorge Carvalho Fernandes
IST, Universidade de Lisboa, Portugal
December 2014

Abstract

Anterior cruciate ligament (ACL) rupture is a serious injury whose frequency has been increasing in the last few years. To understand the causes and consequences of this injury it is fundamental to know the role of the ACL in the knee.

This work aims to analyze the knee behavior after an ACL rupture, through the finite element method. For this purpose, it is used a fully tridimensional model of the tibiofemoral joint, with and without ACL, where loads that evidence the ligament function are applied.

The knee ligaments were modeled with two hyperelastic constitutive models: The isotropic Marlow and the anisotropic Holzapfel-Gasser-Ogden (HGO) models. Both material models were fitted using the same uniaxial stress-strain curves. The parameters of the HGO were estimated with the help of an optimization routine, connecting MATLAB to Abaqus. The comparison between the results obtained through both the constitutive models allows to conclude that HGO model can better reproduce the mechanical behavior of the ligaments.

Despite some verified differences in quantitative terms, the finite element model is able to produce kinematic and force results that confirm the ACL as the main restrainer to anterior tibial (or posterior femoral) translation. Furthermore, in ACL absence, there is a clear increase in knee laxity in more than one degree of freedom, particularly in internal-external tibial rotation.

Keywords: Anterior Cruciate Ligament, Knee Joint, Finite Element Method, Biomechanics.

1. Introduction

The knee joint is the largest and most complex joint in the human body consisting of both femoropatellar and tibiofemoral joints [1]. The structure of the knee permits the bearing of very high loads, as well as the mobility required for locomotor activities [2].

The knee ligaments act as joint stabilizers and movement restrainers [3]. The anterior cruciate ligament (ACL) plays a critical role in the physiological kinematics of the knee joint, being the primary restraint against anterior tibial translation and also limiting knee hyperextension [1,4,5]. ACL rupture is a serious and the most common ligament injury, with an increasing number of 100 000 to 200 000 incidences per year in the United States [6]

A sound knowledge of both biomechanics and kinematics of the knee and the ACL role in it are indispensable to understand the causes of ACL injuries, its consequences, how to prevent them and even to improve surgical procedures. While experimental studies have limitations such as their high cost and low reproducibility, computational models are a good alternative to study several biomechanical quantities with reduced costs and high time and machinery efficiency. In particular, finite element (FE) method analysis can provide accurate and medical relevant results [3,7–9]. The FE simulation technique permits a precise calculation of both special and temporal variations of stresses, strains and contact areas/forces in different situations that can be easily reproduced [8–10]. Therefore, FE analysis are a powerful tool in providing biomechanical information that can be extremely useful in a clinical context.

1.1. Literature Review

The existing computational FE models of the knee, vary in diverse parameters, such as the degree of complexity, the study variables, material models definitions and loading cases. The choice of the parameters to study defines the nature of the analysis, which can be static or quasi-static [3,11,12,7,13–25] or dynamic, [7,26–30].

Due to the intricate anatomy and structure diversity of the knee joint, many of the FE studies simplify the analysis by focusing only on the tibiofemoral joint [11,12,9,16,18,21,23,25,31,32] and by not including parts such as the menisci and the articular cartilage [11,12,9,18,25] or other ligaments [11,12,9,16,25].

Some studies opted for representing the knee ligaments with one-dimensional (1D) truss/beam [13,14,26] or spring [16,17,23,24,30] elements with simplified material properties. Despite the increased ease in obtaining kinematic and force data, this approach does not allow to determine the stress distribution in the ligaments [11,7,33].

When using three-dimensional (3D) representations of the ligaments, the challenge is to develop a material model that can completely characterize the nonlinear behavior of ligaments. To this matter, isotropic [11,12,19,20,33], transversely isotropic [3,9,15,25,32,34] and anisotropic hyperelastic material models [7,31] have been used.

So, it is clear that despite being a widely studied topic on the FE modeling context, the development of a trustworthy model of such a complex structure as the knee joint is a very challenging process. The difficulties increase even more when a good description of the ligaments behavior is required.

1.2. Objectives

The overall goal of this work is to develop a 3D FE model that enables a biomechanical analysis of the knee behavior after an ACL rupture. In detail, this work aims to provide clinical relevant information regarding the force, stress and displacement changes that occur in an ACL deficient knee.

Another objective is to verify the biomechanical changes induced by an isotropic and anisotropic hyperelastic constitutive models in the modeling of the knee ligaments.

It is expected that the model is able to reproduce qualitatively and, if possible, quantitatively the behavior found in the literature in order to form a reliable foundation for futures FE studies regarding the knee joint.

2. Methods

The knee joint geometry used in this thesis was obtained from the Open Knee project. [35,36]. This includes 3D solid representations of eleven parts of the tibiofemoral joint: distal femur, proximal tibia, articular cartilages (femoral, medial tibial, and lateral tibial), anterior cruciate ligament (ACL), posterior cruciate ligament (PCL), medial collateral ligament (MCL) and lateral collateral ligament (LCL) and the medial and lateral menisci.

The bones were defined as rigid bodies due to their much greater stiffness in comparison to soft tissues and meshed with quadrilateral and triangular shell elements. The remaining tissues were meshed with hexaedral (C3D8) elements.

Articular cartilage was modeled as linear elastic isotropic material. Despite being a hydrated tissue, the time of interest of the loading cases discussed in this thesis is too small compared to the viscoelastic time constant of cartilage (1 s versus 1500 s), making this a reasonable approximation. The same approach has been adopted in many other studies [3,7,14,16,17,19–22,26,30]. From the different values available in the literature, the Young's modulus (*E*) and Poisson's ratio (υ) of the articular cartilage were chosen to be 5 MPa [3,17,21,22] and 0.46 [3,21], respectively. The same explanation goes for the menisci, for which was assumed *E*=59 MPa and υ=0.49 [3,21]. The viscoelastic behavior of the ligaments was also neglected. However, considering their highly non-linear stress-strain behavior and the information found in the literature with respect to their material modeling, it would be too simplistic to describe the ligaments with linear elastic properties. Therefore, two hyperelastic constitutive models available in the material set library of Abaqus were tested: the Marlow and the Holzapfel-Gasser-Ogden (HGO) constitutive models.

The Marlow model, developed by R.S. Marlow [37], is a general first-invariant hyperelastic constitutive model, whose strain energy density function Ψ (SEDF) depends exclusively on the first-invariant, I and is presented in Eq. 1.

$$\Psi(\bar{I}_1) = \int_0^{\lambda_T(\bar{I}_1)-1} T(\varepsilon)\, d\varepsilon \qquad (1)$$

Where $T(\varepsilon)$ is the nominal uniaxial traction, $\lambda_T(\bar{I}_1)$ is the uniaxial stretch and ε is the uniaxial strain. The incompressibility constraint is introduced by $\bar{I}_1$, which is the isochoric part of the first strain invariant, I_1.

To adjust this model to a given stress-strain curve in Abaqus (Simulia, Providence, USA), we need only to provide the experimental stress-strain data points, which will substitute the term T and, therefore, there is no need

of a curve-fitting procedure. By doing this, the curve created by the modelwill pass in each of the points given, reproducing exactly the stress-strain behavior used in its definition.

The HGO constitutive model was developed by Gasser et al. [38] to describe the histology and mechanical properties of arterial tissue. By adding a scalar parameter to account for the dispersion of collagen fibers to a previous structural framework [39,40], they defined a model especially suited to describe the anisotropic hyperelastic behavior of collagen fiber reinforced materials, such as the ligaments. Considering that the material to model consists of two families of fibers, each of the families can be characterized by a mean referential (preferred) direction about which the fibers are distributed with rotational symmetry. The two distinct directions in the reference configuration are defined in terms of two unit vectors $\boldsymbol{a}_{0i}, i = 4{,}6$. This allows the definition of two additional invariants:

$$I_4 = \boldsymbol{a}_{04} \cdot (\boldsymbol{C}\boldsymbol{a}_{04}), \qquad I_6 = \boldsymbol{a}_{06} \cdot (\boldsymbol{C}\boldsymbol{a}_{06}) \tag{2}$$

With these concepts in mind, the SEDF of the HGO model for the incompressible case is presented in Eq. (3):

$$\Psi = C_{10}(\bar{I}_1 - 3) + \frac{k_1}{k_2}\sum_i^N \left\{e^{k_2(\bar{E}_i)} - 1\right\} \tag{3}$$

Where,

$$\bar{E}_i \overset{\text{def}}{=} \kappa(\bar{I}_1 - 3) + (1 - 3\kappa)(\bar{I}_{(i)} - 1) \tag{4}$$

The first term in Eq. (3) serves to model the non-collagenous ground matrix by means of a neo-Hookean incompressible isotropic model while the second term accounts for the families of fibers with different directions embedded in the ground matrix.

$N\ (\leq 3)$ is the number of fiber families. For $N = 2$, we can set $i = 4{,}6$ and the term $\bar{I}_{(i)}$ can be substituted in Eq. (4) by the isochoric parts of the invariants defined in Eq. (2).

C_{10}, D, k_1, k_2 are the parameters of the model that change the stress-strain response to model different materials.

κ is the parameter that controls the dispersion around the mean direction of each family of fibers. When $\kappa = 0$, the fibers are perfectly aligned in the preferential direction. As the value increases, the fiber dispersion also increases until κ reaches $1/3$, which represents randomly distributed fibers (isotropic situation).

The application of the HGO model implies the definition of a preferential direction for the fibers. To implement this direction, a continuous element-by-element orientation was defined for each ligament as in [31]. The result of this procedure is depicted in Figure 1 where the variation of the local X-axis along the longitudinal axis of the PCL can be seen.

The collateral ligaments were modeled with just one family of fibers along the longitudinal direction, using the procedure just indicated.

The cruciate ligaments, however, are commonly described has being composed of two distinct fiber bundles. To recreate the anteromedial (AM) and posterolateral (PL) family fibers of the ACL, the two vectors $(\boldsymbol{a}_{0i}, i = 4{,}6)$ governing the two different directions of each fiber family were defined resorting to a γ value that defined an angle with the local x-axis in the local xy plane. By setting the γ value equal to 10º, the x-component of the first local material direction with respect to the coordinate system (CS) defined at a given element is $\cos\gamma$, while the y-component is $\sin\gamma$. Similarly, the x and y components of the second local material direction are given by $\cos\gamma$ and $\sin -\gamma$, respectively. The local coordinate system and local directions in the xy plane are schematically represented in Figure 2.

The estimation of the model parameters was performed through an optimization routine that used Python instructions to connect MATLAB (The MathWorks Inc., Natick, MA, USA) to Abaqus. The objective of this optimization routine was to reproduce the experimental nominal stress-strain curves of uniaxial tests presented in [21] for the ACL, [41] for the MCL, and [42] for the PCL.

Preliminary analyses revealed discrepancies in stress distribution in the proximal portion of the ACL, the "ACL head", which had to modeled as an isotropic material by setting $\kappa = 1/3$.

The whole optimization process is presented schematically in Figure 3 and the final set of parameters is summarized in Table 1.

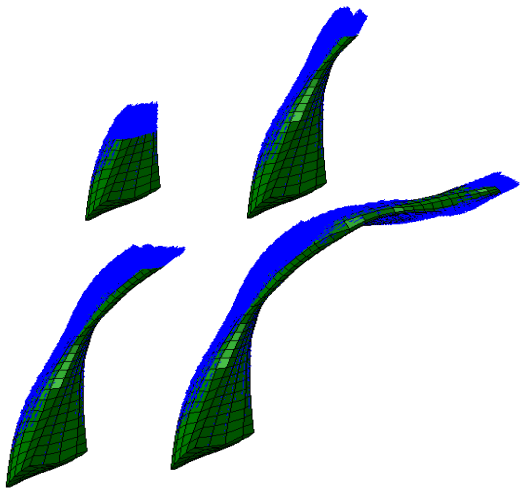

Figure 1 - Main PCL fiber direction. The blue lines represent the direction of the x-axis in the local coordinate system of each element.

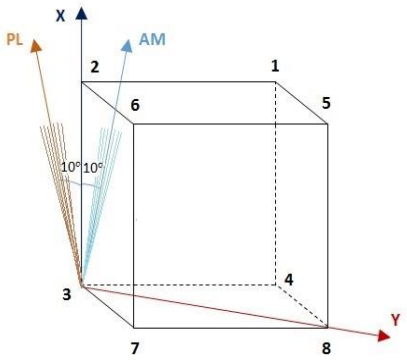

Figure 2 - Schematic representation of the local coordinate system used in each element of the ACL to define the direction of the two fiber families. Considering the planes 567, 145 and 236 as the anterior, medial and lateral planes, the AM and PL bundles of the ACL can be defined in the local coordinate system represented. The smaller lines around the AM and PL directions represent the dispersion of the collagen fibers direction, controlled by the κ parameter.

Eleven locations of potential contact were identified (femoral cartilage to tibial cartilage, cartilages to menisci, ligaments to bones and ACL to PCL.). Each contact pair interaction was defined as *Surface-to-Surface Contact* with frictionless finite sliding between each contact pair as in [3,7,16,17,21,22].

2.1. Loads and Boundary Conditions

The model was aligned with a coordinate system (CS) consistent with a CS commonly used to describe the tibiofemoral joint movements. In this CS, origin is defined as the mid-point of the femoral condyles, the x-axis is flexion axis, the y-axis is the anterior-posterior axis and the z-axis represents the mechanical axial axis.

A posterior load of 134 N was applied to the healthy knee, in the *Reference Point* (RP) that controlled the rigid body motion of the femur at 0, 15 and 30º of flexion.

Due to the large displacements of the femur in ACL absence, the value of the force applied in the ACL-deficient knee was reduced to half.

These loading conditions were designed to simulate clinical examinations used to diagnose ACL deficiency, such as the Lachman test [43] and to compare the knee kinematics at different angles of flexion with the experimental data.

During the application of the force, the flexion-extension degree of freedom (DOF) of the femur was fixed and the tibia was fixed in all DOFs. Therefore, the posterior displacement of the femur relative to the tibia is equivalent to the anterior tibial translation relative to the femur that happens during clinical evaluations of the ACL function.

Each of the distal ends of the four ligaments were constrained to a different RP by a *Kinematic Coupling* constraint. These reference points were fixed in all degrees of freedom. In this way, the reaction force measured on each RP would represent the *in situ* force taken up by each ligament in response to tibial motion.

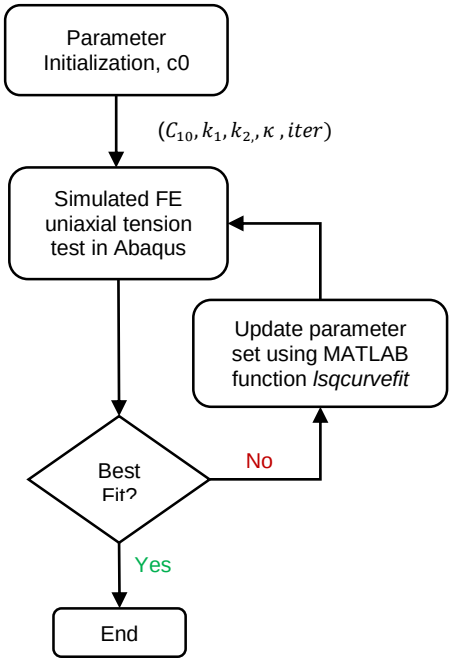

Figure 3 - Diagram of the optimization process of the HGO model parameters. Adapted from [48].

Table 1 - Final set of parameters of the HGO model for each ligament.

	C_{10}/MPa	k_1/MPa	k_2	κ	Fiber Fam.
ACL (body)	0.117	30.779	8.411	0.066	2
ACL (head)	20.000	2912.833	0.100	1/3	2
PCL	0.011	7.826	446.198	0.057	2
MCL & LCL	0.213	61.344	18.706	0.085	1

3. Results and Discussion

For each of the flexion angles mentioned, the results presented are: the kinematic results in terms of tibial relative displacement; the magnitude of the reaction force at the tibial insertion of each ligament and the

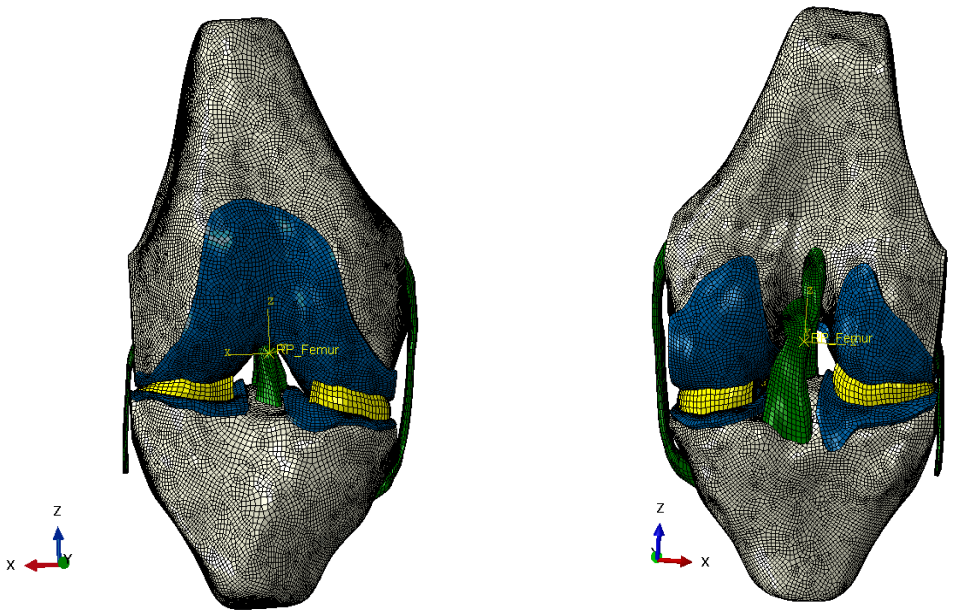

Figure 4 - Mesh of the fully assembled knee aligned with the new coordinate system and with the femoral RP highlighted. Different colors represent different tissues: grey for bones, blue for articular cartilages, yellow for menisci and green for ligaments. (Left) Anterior view. (Right) Posterior view.

maximum principal stress at each ligament, calculated as an average of the nodal stresses of the corresponding ligament. For the case where the knee is at 30º of flexion, both anterior (or lateral, in the ACL-deficient knee) and medial views of the tibiofemoral joint are also presented, showing the maximum principal stress of the soft tissues.

The comparison between the two materials models was made only for the knee in full extension. For higher flexion angles, only the HGO model was considered.

3.1. ACL-Intact Knee

3.1.1. Full Extension (0º of Flexion)

The kinematic, force and stress results for the ACL-intact knee at full extension using both material models are presented in Figure 5 and Table 2, respectively.

Table 2 - Ligaments reaction force and average maximum principal stress in the ACL-intact knee at full extension under a 134 N posterior femoral force.

		ACL	LCL	MCL	PCL
Reaction Force (Mag.) /N	**HGO**	133.200	0.757	7.906	0.007
	Marlow	121.719	5.844	13.037	3.228
Avg. Max. Princ. Stress /MPa	**HGO**	11.350	0.130	0.578	0.001
	Marlow	10.000	1.368	0.967	0.290

The comparison between the two material models shows that with the Marlow model, there is less movement in all DOFs. This was an expected result, since this model defines the ligaments as isotropic materials, and consequently, their resistance to longitudinal and transverse loads is the same, thus providing more restrain in each direction.

This behavior is also expressed by the forces taken up by each ligament. In the Marlow model, the ACL is less loaded than in the HGO model and the contrary happens to the other ligaments due to their ability to sustain loads in directions other than in the longitudinal one. The simulations with the HGO model show a better agreement with the experimental data than the simulations with the Marlow model, with all the displacements falling in the region delimited by the standard deviation. The exception to this is the distal translation (U3), which is slightly above the superior limit of the standard deviation.

For a more reliable model validation, it is mentioned the experimental data obtained by other authors when applying the same 134 N force. For anterior tibial translation, the values obtained by Yagi et. [44], Song et al. [12] and Kanamori et al. [45] were, respectively, 4.1 ± 0.6, 4.6 and 5.3 ± 1 mm. For internal rotation of the tibia, Song et al. reports 1.6º while Kanamori et al. refers 2.1 ± 3.1º.The anterior tibial translation obtained in the FE simulation was less than the experimental average values, which might suggest that the ACL was modeled a bit too stiffer than it should be. This topic is further discussed in the following sections.

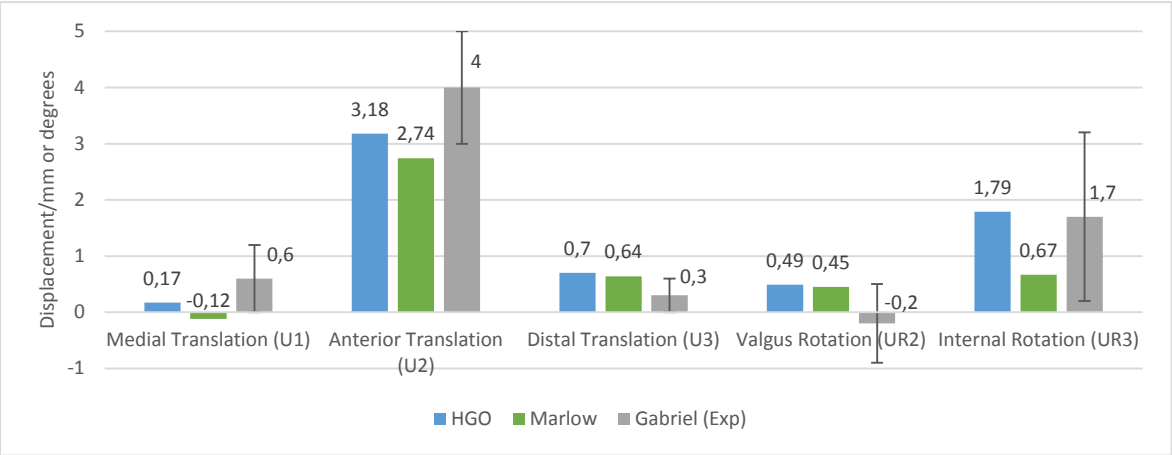

Figure 5 - Kinematic results of relative tibial movement under a 134 N posterior femoral load at full extension. The results of the simulation are compared to the experimental data of Gabriel et al *[43]*.

Regarding the ACL *in situ* force, all the three experimental studies above mentioned report values between 115 and 140 N, validating the value of 133.2 N obtained in the simulations.

As for the ligament stresses, there was not much data available in the literature. In experimental tests using cadaveric knees it is difficult to accurately measure the stress. In the case of FE studies, the lack of data is related to the fact that many of them use one dimensional (truss/beam or spring) elements to model the ligaments, which cannot give stress information. Nevertheless, the values obtained for the ACL seem to be within the range of values reported in two FE studies simulating similar loading conditions: Peña et al. [3] obtained an average maximal principal stress of 6.5 MPa for the ACL and a maximum value of 15 MPa, while Song et al. [12] obtained an average value of 6.9 MPa and a maximum value of 24 MPa.

3.1.2. 15º of Flexion

The kinematic, force and stress results for the ACL-intact knee at 15º of flexion using the HGO model are presented in Figure 6 and Table 3, respectively.

Table 3 - Ligaments reaction force and average maximum principal stress in the ACL-intact knee at 15º of flexion under a 134 N posterior femoral force.

	ACL	LCL	MCL	PCL
Reaction Force (Magnitude)/N	136.732	1.322	5.998	0.011
Avg. Max. Principal Stress/MPa	11.724	0.198	0.436	0.002

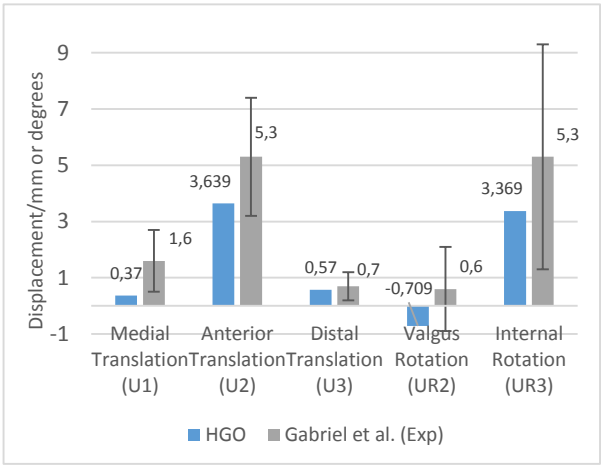

Figure 6 - Kinematic results of relative tibial movement under a 134 N posterior femoral load at 15º of flexion using the HGO model in the ligaments. The results of the simulation are compared to the experimental data of Gabriel et al [43].

3.1.3. 30º of Flexion

The kinematic, force and stress results for the ACL-intact knee at full extension using the HGO model are presented in Figure 8Figure 6 and Table 4, respectively. For this flexion angle, a picture of the full knee is also presented in Figure 7, showing the maximum principal stresses of the knee soft tissues.

Table 4 - Ligaments reaction force and average maximum principal stress in the ACL-deficient knee at 30º of flexion under a 134 N posterior femoral force.

	ACL	LCL	MCL	PCL
Reaction Force (Magnitude)/N	138.634	9.783	5.876	0.018
Avg. Max. Principal Stress/MPa	11.724	1.459	0.409	0.003

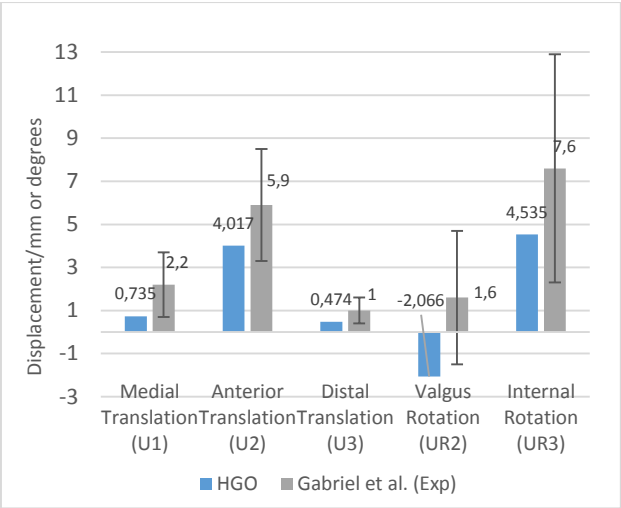

Figure 8 - Kinematic results of relative tibial movement under a 134 N posterior femoral load at 30º of flexion using the HGO model in the ligaments. The results of the simulation are compared to the experimental data of Gabriel et al [43].

At 30º, the FE kinematic results (Figure 8) are again in accordance to the experimental data of Gabriel et al, except for the valgus rotation. Both anterior tibial translation and internal rotation continue to increase as the flexion angle goes from 15 to 30º. This is concomitant with the higher force magnitude of the ACL, which is more requested as the flexion angle increases (in the range of flexion considered). At this angle of flexion, Yagi et al. [44] and Kanamori et al. [45] obtained an anterior tibial displacement of 6.4 ± 2.4 mm and 10.1 ± 3.8 mm, respectively. For the ACL *in situ* force, the same authors report values ranging from 106 to 155 N.

By comparing the simulation results with all sets of experimental data for this flexion angle, we can again verify that the model underpredicts anterior tibial translation, supporting the hypothesis of increased ACL stiffness posed earlier.

Making a global analysis of the results obtained for the ACL-intact knee, it is reasonable to say that the model provides kinematic outputs that are qualitatively (and mostly quantitatively) consistent with the experimental data except for the valgus-varus rotation. The remaining DOFs, despite some differences in terms of absolute values (as it happens with the underprediction of the anterior tibial movement) are almost always within the range of values indicated and tend to follow the behavior reported in the literature.

The results of the ACL *in situ* forces are also in good agreement with the literature values. For the other ligaments, the only data found was again from Kanamori et al [45] which reports values between 14 and 15 N for the MCL *in situ* forces for all the range of flexion here considered. The obtained values were lower than this. While on one hand this could also point to some change to be made to the ligament properties, on the other hand, it would be interesting to have more experimental data on this matter to draw more solid conclusions.

The validity of the stress results is more difficult to evaluate due to the lack of experimental data, but when in comparison to similar FE simulations, the obtained average values seem to be in the correct interval of values, at least when the knee is in full extension.

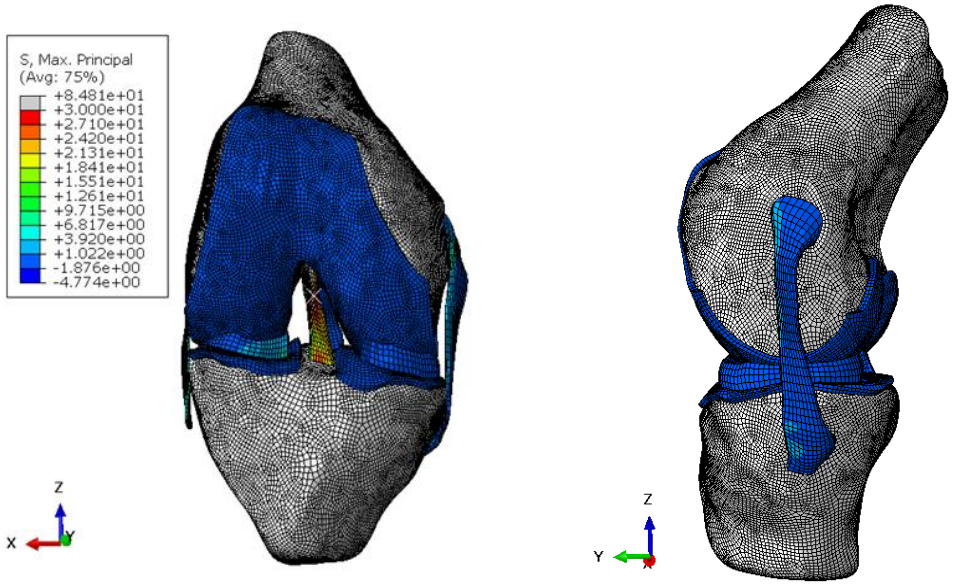

Figure 7 - ACL-intact knee joint at 30º of flexion after the application of a 134 N posteriorly directed force on the femur using the HGO material model in the ligaments. (Left side) Anterior view. (Right side) Medial view.

3.2. ACL-Deficient Knee

3.2.1. Full Extension (0º of Flexion)

The kinematic, force and stress results for the ACL-deficient knee at full extension, using both material models are presented in Figure 9 and Table 5, respectively.

Table 5 - Ligaments reaction force and average maximum principal stress in the ACL-intact knee at full extension under a 67 N posterior femoral force - comparison between the two material models.

		LCL	MCL	PCL
Reaction Force (Mag.)/N	**HGO w/ ACL**	0.279	4.737	0.014
	HGO w/o ACL	65.233	70.294	0.014
	Marlow w/ ACL	2.513	7.348	1.342
	Marlow w/o ACL	41.957	48.57	7.359
Avg. Max. Princ. Stress/MPa	**HGO w/ ACL**	0.051	0.351	0.001
	HGO w/o ACL	10.851	5.023	0.004
	Marlow w/ ACL	0.716	0.551	0.115
	Marlow w/o ACL	8.275	3.485	0.787

3.2.2. 15º of Flexion

The kinematic, force and stress results for the ACL-deficient knee at full extension, using the HGO model are presented in Figure 10 and Table 6, respectively.

Table 6 - Ligaments reaction force and average maximum principal stress in the ACL-deficient knee at 15º of flexion under a 67 N posterior femoral force.

		LCL	MCL	PCL
Reaction Force (Magnitude) /N	**w/ ACL**	2.480	5.759	0.019
	w/o ACL	67.556	75.001	0.019
Avg. Max. Principal Stress/MPa	**w/ ACL**	0.376	0.419	0.001
	w/o ACL	11.000	5.370	0.002

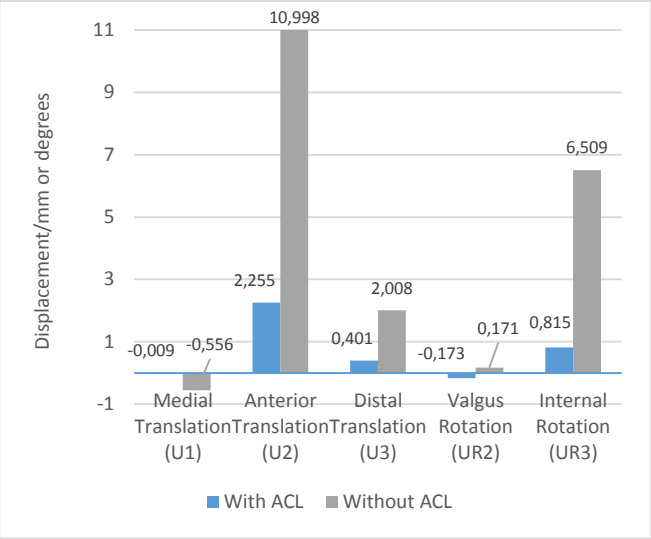

Figure 10 - Kinematic results of relative tibial movement under a 67 N posterior femoral load at 15º of flexion using the HGO model in the ligaments - comparison between the ACL-intact and ACL-deficient knees.

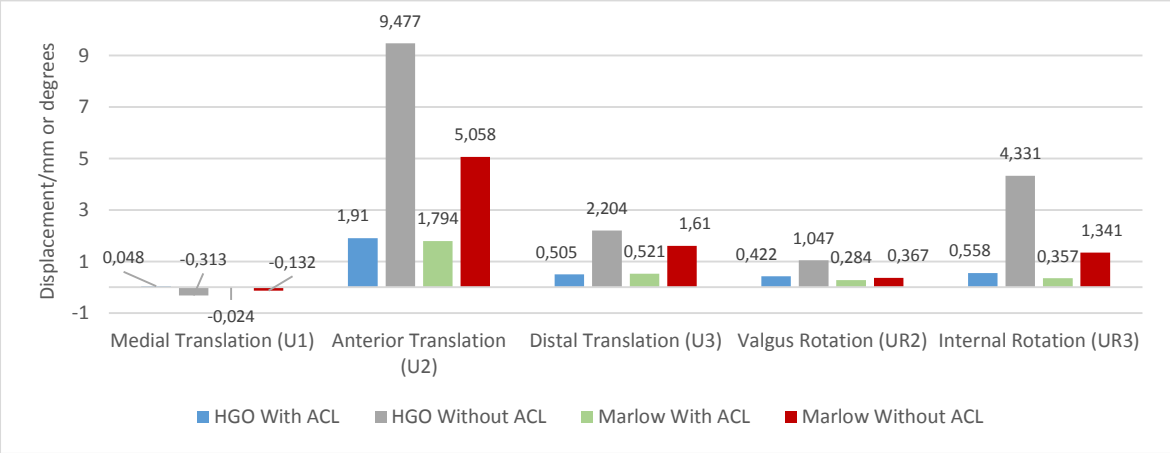

Figure 9 - Kinematic results of relative tibial movement under a 67 N posterior femoral load at full extension in ACL-intact and ACL-deficient knees – comparison between the two material models.

3.2.1. 30º of Flexion

The kinematic, force and stress results for the ACL-deficient knee at full extension using the HGO model are presented in Figure 11 and Table 7, respectively. For this flexion angle, a picture of the full knee is also presented in Figure 12, showing the maximum principal stresses of the soft tissues.

Table 7 - Ligaments reaction force and average maximum principal stress in the ACL-deficient knee at 30º of flexion under a 67 N posterior femoral force.

		LCL	MCL	PCL
Reaction Force (Magnitude) /N	**w/ ACL**	12.253	7.514	0.013
	w/o ACL	70.598	77.786	0.026
Avg. Max. Principal Stress/MPa	**w/ ACL**	1.855	0.532	0.002
	w/o ACL	11.228	5.531	0.004

With the increase of the flexion angle, the kinematic results show the same growing trend in both anterior tibial translation and internal rotation seen in the first set of simulations with the ACL-intact knee, demonstrating the clear impact of the ACL in these DOFs. When comparing Figure 7 with Figure 12 we can clearly observe a much larger displacement in the latter case. The lack of the ACL is compensated by the collateral ligaments, whose stress increased largely, as expected. The anterior region of these ligaments is easily identified as the region of higher stresses.

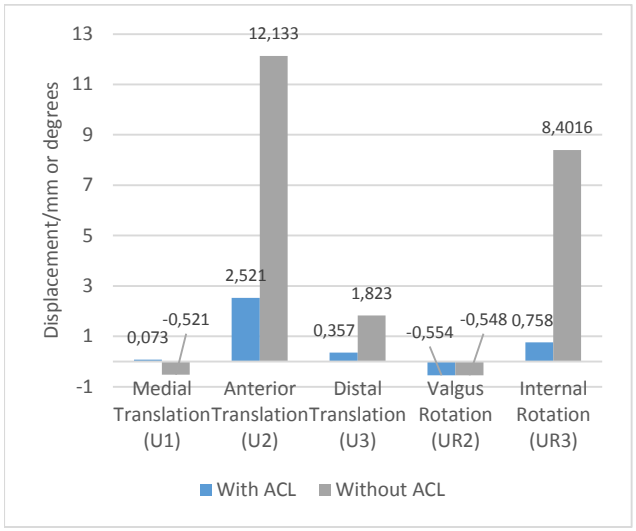

Figure 11 - Kinematic results of relative tibial movement under a 67 N posterior femoral load at 30º of flexion using the HGO model in the ligaments - comparison between the ACL-intact and ACL-deficient knees.

Despite the decrease in distal translation with the increase of the flexion angle, the knee without the ACL always presents a higher value than the knee with the ACL, which also suggests the importance of the ACL in this proximal-distal direction.

Given that the experimental studies on cadaveric knees can apply the same 134 N anterior load on the tibia, the simulated results had to be compared with this data, taking into account the difference in the value of the applied load.

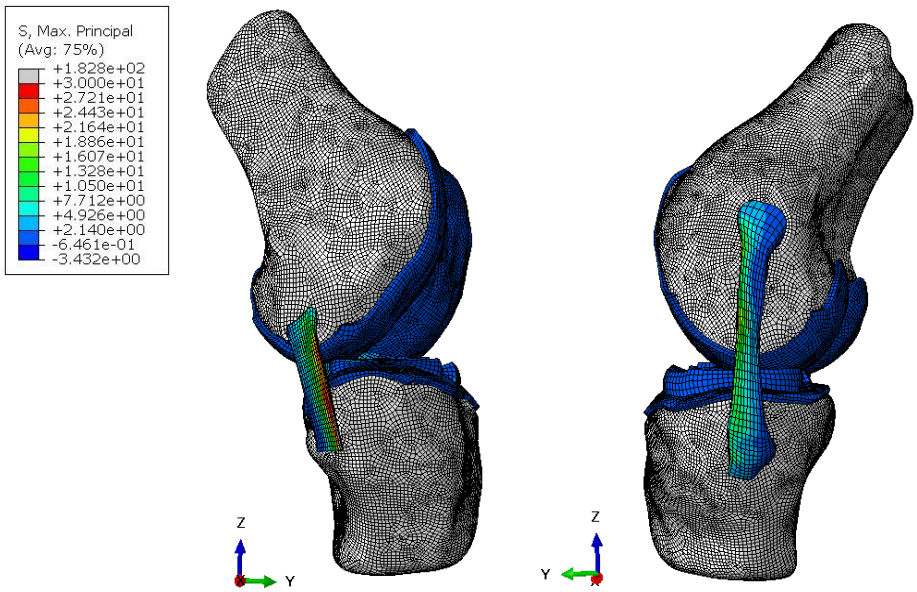

Figure 12 - ACL-deficient knee joint at 30º of flexion after the application of a 67 N posteriorly directed force on the femur using the HGO material model in the ligaments. (Left side) Lateral view. (Right side) Medial view.

For the 134 N anterior load, Kanamori et al. [45] obtained an anterior tibial displacement of 13.3±1.4, 17.3±1.8 and 18.9±2.3 mm in the ACL-deficient knee at 0, 15 and 30º of flexion, respectively. Similar results were acquired by Yagi et al. [44] with approximately 12.5 and 19 mm for 0 and 30º of flexion, respectively.

In terms of the *in situ* forces, Kanamori et al. verified that after the ACL transection the *in situ* forces of the MCL increase significantly from less than 20 N in the ACL-intact knee case to 36 ± 27 N and 41±16 N at 0 and 30º of flexion, respectively.

Since the value of the applied force in the FE simulation was only half of the value applied in the experimental studies mentioned, it seems that the FE model overpredicts the anterior tibial displacement when the ACL is removed, as well as the *in situ* forces in the MCL This fact, associated with the underprediction of movement for the same DOF when the ACL is present, suggests a revision of the ligament properties. For example, if the stiffness of the collateral ligaments was increased while the stiffness of the ACL was decreased, the FE simulation should produce a higher anterior tibial movement when the ACL is present and a lower value of the same quantity when the ACL is removed.

The stress-strain properties of the ligaments can greatly vary with the strain rate at which the uniaxial tension tests are preformed, as we can attest in [46]. Therefore, one way to try to improve the results would be to perform the curve fitting procedure to other experimental stress-strain curves with requirements described above.

4. Conclusion

In this work, the effect of an ACL rupture in the overall kinematics and biomechanics of the knee was studied by comparing the effect of a posterior femoral force on ACL-intact and ACL-deficient knees.

By comparing the kinematic outcomes of the FE simulations with two material models, it is concluded that the HGO model presents more accurate results. This was expected since the HGO was designed to capture the anisotropic properties of biologic tissues composed of collagen fiber bundles, such as the ligaments.

Using this model in the ligaments, the FE model is able to qualitatively (and mostly quantitatively) reproduce consistent kinematic results with experimental data in all degrees of freedom except for the valgus-varus rotation. These results confirm that the ACL provides the major constraint to anterior tibial motions and also plays an important role on restraining internal rotation of the tibia. These conclusions are also supported by the calculated force sustained by the four ligaments considered.

When the ACL is absent, the collateral ligaments are the first structures to be requested to sustain anterior-posterior forces, with obvious implications in their stress state. The MCL is the ligament that supports more load in this situation, in accordance to the role attributed to the MCL as the secondary restraint to anterior tibial displacements.

To sum up, it is concluded that the ACL rupture induces several drastic kinematic changes which have a great impact on the overall biomechanics of the entire knee structure.

As usual in this type of simulations, there were some limitations to this study. For instance, the residual stresses present on the knee ligaments were not modeled since the Abaqus does not allow the prescription of pre-stresses in anisotropic hyperelastic models. Other shortcoming was that the ACL function was only tested by applying a posterior femoral load. The influence of the ACL in other types of movements was not tested.

Despite these limitations, the FE model developed in this thesis, based on the overall positive results produced, should provide a solid basis to further develop significant work in the biomechanical study of the knee.

In the future, an obvious addition to the model would be the inclusion of the patellofemoral component. The meniscal attachments to the tibia could also be more realistically modeled by defining the meniscal horns as a set of springs as in [16,22,31].

As for the knee ligaments modeling, it is known that the ligaments are not completely incompressible tissues. In a very recent study, Nolan et al. [47] demonstrated that the HGO model does not correctly characterizes the compressible anisotropic material behavior. In response to this fact, they proposed a modified anisotropic model based on the aforementioned model that is said to predict more accurately the anisotropic response to hydrostatic tensile loading. The employment of this new model would require an additional effort to implement an UMAT routine in Abaqus, but would also add an extra layer of realism to the ligaments material properties.

Finally, it would be interesting to verify the ACL role in more complex loading cases. The simulation of more dynamic situations like jumping or stair climbing together with a more detailed analysis of the other soft tissues of the knee, such as the articular cartilage and the menisci, would also provide great insights about the ACL-deficient knee functioning.

5. References

[1] Marieb, E., and Hoehn, K., 2013, Human anatomy & physiology, Pearson Education, Inc.

[2] Hall, S., 2012, Basic Biomechanics, McGraw-Hill, New York, NY.

[3] Peña, E., Calvo, B., Martínez, M. a, and Doblaré, M., 2006, “A three-dimensional finite element analysis of the combined behavior of ligaments and menisci in the healthy human knee joint.,” J. Biomech., **39**(9), pp. 1686–1701.

[4] Dargel, J., Gotter, M., Mader, K., Pennig, D., Koebke, J., and Schmidt-Wiethoff, R., 2007, “Biomechanics of the anterior cruciate ligament and implications for surgical reconstruction,” Strategies Trauma Limb Reconstr., **2**(1), pp. 1–12.

[5] Kweon, C., Lederman, E. S., and Chhabra, A., 2013, “Anatomy and Biomechanics of the Cruciate Ligaments and Their Surgical Implications,” The Multiple Ligament Injured Knee: A Practical Guide to Management, G.C. Fanelli, ed., Springer New York, New York, NY, pp. 17–27.

[6] Siegel, L., Vandenakker-Albanese, C., and Siegel, D., 2012, “Anterior Cruciate Ligament Injuries: Anatomy, Physiology, Biomechanics, and Management.,” Clin. J. Sport Med. Off. J. Can. Acad. Sport Med., **22**(4), pp. 349–355.

[7] Kiapour, A., Kiapour, A. M., Kaul, V., Quatman, C. E., Wordeman, S. C., Hewett, T. E., Demetropoulos, C. K., and Goel, V. K., 2014, “Finite Element Model of the Knee for Investigation of Injury Mechanisms: Development and Validation,” J. Biomech. Eng., **136**(1), p. 011002.

[8] Herrera, A., Ibarz, E., Cegoñino, J., Lobo-Escolar, A., Puértolas, S., López, E., Mateo, J., and Gracia, L., 2012, “Applications of finite element simulation in orthopedic and trauma surgery.,” World J. Orthop., **3**(4), pp. 25–41.

[9] Gardiner, J. C., and Weiss, J. a, 2003, “Subject-specific finite element analysis of the human medial collateral ligament during valgus knee loading.,” J. Orthop. Res., **21**(6), pp. 1098–1106.

[10] Kluess, D., Wieding, J., and Souffrant, R., “x Finite Element Analysis in Orthopaedic Biomechanics,” pp. 151–171.

[11] Xie, F., Yang, L., Guo, L., Wang, Z., and Dai, G., 2009, “A Study on Construction Three-Dimensional Nonlinear Finite Element Model and Stress Distribution Analysis of Anterior Cruciate Ligament,” J. Biomech. Eng., **131**(12), pp. 121007–5.

[12] Song, Y., Debski, R. E., Musahl, V., Thomas, M., and Woo, S. L.-Y., 2004, “A three-dimensional finite element model of the human anterior cruciate ligament: a computational analysis with experimental validation,” J. Biomech., **37**(3), pp. 383–390.

[13] Adouni, M., Shirazi-Adl, A., and Shirazi, R., 2012, “Computational biodynamics of human knee joint in gait: from muscle forces to cartilage stresses.,” J. Biomech., **45**(12), pp. 2149–2156.

[14] Bendjaballah, M., Shirazi-Adl, A., and Zukor, D., 1997, “Finite element analysis of human knee joint in varus-valgus,” Clin. Biomech., **12**(3), pp. 139–148.

[15] Dhaher, Y. Y., Kwon, T.-H., and Barry, M., 2010, “The effect of connective tissue material uncertainties on knee joint mechanics under isolated loading conditions.,” J. Biomech., **43**(16), pp. 3118–3125.

[16] Hull, M. L., Donahue, T., Rashid, M., and Jacobs, C., 2002, “A Finite Element Model of the Human Knee Joint for the Study of Tibio-Femoral Contact,” J. Biomech. Eng., **124**(3), pp. 273–280.

[17] Li, G., Gil, J., Kanamori, A., and Woo, S. L., 1999, “A validated three-dimensional computational model of a human knee joint.,” J. Biomech. Eng., **121**(6), pp. 657–662.

[18] Park, H.-S., Ahn, C., Fung, D. T., Ren, Y., and Zhang, L.-Q., 2010, “A knee-specific finite element analysis of the human anterior cruciate ligament impingement against the femoral intercondylar notch.,” J. Biomech., **43**(10), pp. 2039–2042.

[19] Ramaniraka, N. a, Saunier, P., Siegrist, O., and Pioletti, D. P., 2007, “Biomechanical evaluation of intra-articular and extra-articular procedures in anterior cruciate ligament reconstruction: a finite element analysis.,” Clin. Biomech. (Bristol, Avon), **22**(3), pp. 336–343.

[20] Ramaniraka, N. a, Terrier, A., Theumann, N., and Siegrist, O., 2005, “Effects of the posterior cruciate ligament reconstruction on the biomechanics of the knee joint: a finite element analysis.,” Clin. Biomech. (Bristol, Avon), **20**(4), pp. 434–442.

[21] Wan, C., Hao, Z., and Wen, S., 2013, “The Effect of the Variation in ACL Constitutive Model on Joint Kinematics and Biomechanics Under Different Loads: A Finite Element Study,” J. Biomech. Eng., **135**(4), p. 041002.

[22] Yao, J., Snibbe, J., Maloney, M., and Lerner, A. L., 2006, “Stresses and Strains in the Medial Meniscus of an ACL Deficient Knee under Anterior Loading: A Finite Element Analysis with Image-Based Experimental Validation,” J. Biomech. Eng., **128**(1), p. 135.

[23] Moglo, K. E., and Shirazi-Adl, a., 2003, “Biomechanics of passive knee joint in drawer: load transmission in intact and ACL-deficient joints,” Knee, **10**(3), pp. 265–276.

[24] Li, G., Suggs, J., and Gill, T., 2002, “The Effect of Anterior Cruciate Ligament Injury on Knee Joint Function under a Simulated Muscle Load: A Three-Dimensional Computational Simulation,” Ann. Biomed. Eng., **30**(5), pp. 713–720.

[25] Ellis, B. J., Lujan, T. J., Dalton, M. S., and Weiss, J. A., 2006, “Medial Collateral Ligament Insertion Site and Contact Forces in the ACL-Deficient Knee,” J. Orthop. Res., (April), pp. 800–810.

[26] Penrose, J. M. T., Holt, G. M., Beaugonin, M., and Hose, D. R., 2002, “Development of an accurate three-dimensional finite element knee model.,” Comput. Methods Biomech. Biomed. Engin., **5**(4), pp. 291–300.

[27] Baldwin, M. a, Clary, C. W., Fitzpatrick, C. K., Deacy, J. S., Maletsky, L. P., and Rullkoetter, P. J., 2012, “Dynamic finite element knee simulation for evaluation of knee replacement mechanics.,” J. Biomech., **45**(3), pp. 474–483.

[28] Halloran, J. P., Petrella, A. J., and Rullkoetter, P. J., 2005, “Explicit finite element modeling of total knee replacement mechanics.,” J. Biomech., **38**(2), pp. 323–331.
[29] Godest, a C., Beaugonin, M., Haug, E., Taylor, M., and Gregson, P. J., 2002, “Simulation of a knee joint replacement during a gait cycle using explicit finite element analysis.,” J. Biomech., **35**(2), pp. 267–275.
[30] Beillas, P., Papaioannou, G., Tashman, S., and Yang, K. H., 2004, “A new method to investigate in vivo knee behavior using a finite element model of the lower limb.,” J. Biomech., **37**(7), pp. 1019–1030.
[31] Westermann, R. W., Wolf, B. R., and Elkins, J. M., 2013, “Effect of ACL reconstruction graft size on simulated Lachman testing: a finite element analysis.,” Iowa Orthop. J., **33**, pp. 70–77.
[32] Peña, E., Martínez, M. a, Calvo, B., Palanca, D., and Doblaré, M., 2005, “A finite element simulation of the effect of graft stiffness and graft tensioning in ACL reconstruction.,” Clin. Biomech. (Bristol, Avon), **20**(6), pp. 636–644.
[33] Pioletti, D., Rakotomanana, L., Benvenuti, J., and PF, L., 1998, “Finite Element Model of the Human Anterior Cruciate Ligament,” Comput. methods Biomech. Biomed. Eng.
[34] Limbert, G., Taylor, M., and Middleton, J., 2004, “Three-dimensional finite element modelling of the human ACL: simulation of passive knee flexion with a stressed and stress-free ACL.,” J. Biomech., **37**(11), pp. 1723–1731.
[35] Erdemir, A., and Sibole, S., 2010, “Open Knee : A Three Dimensional Finite Element Representation of the Knee Joint, User’s Guide, Version 1.0.0.”
[36] https://simtk.org/home/openknee, “Simtk.org: Open Knee: A ThreeDimensional Finite Element Representation of the Knee Joint.”
[37] Marlow, R. S., 2003, “A General First-Invariant Hyperelastic Constitutive Model,” Constitutive Models for Rubber III, pp. 157–160.
[38] Gasser, T. C., Ogden, R. W., and Holzapfel, G. a, 2006, “Hyperelastic modelling of arterial layers with distributed collagen fibre orientations.,” J. R. Soc. Interface, **3**(6), pp. 15–35.
[39] Holzapfel, G. A., Gasser, T. C., and Ogden, R. A. Y. W., 2000, “A New Constitutive Framework for Arterial Wall Mechanics and a Comparative Study of Material Models,” J. Elast., **61**, pp. 1–48.
[40] Holzapfel, G., and Gasser, T., 2001, “A viscoelastic model for fiber-reinforced composites at finite strains: Continuum basis, computational aspects and applications,” Comput. methods Appl. Mech. …, **190**, pp. 4379–4403.
[41] Quapp, K., and Weiss, J., 1998, “Material characterization of human medial collateral ligament,” ASME J. Biomech. Eng.
[42] Butler, D. L., Sheh, M. Y., Stouffer, D. C., Samaranayake, V. a, and Levy, M. S., 1990, “Surface strain variation in human patellar tendon and knee cruciate ligaments.,” J. Biomech. Eng., **112**(1), pp. 38–45.
[43] Gabriel, M. T., Wong, E. K., Woo, S. L.-Y., Yagi, M., and Debski, R. E., 2004, “Distribution of in situ forces in the anterior cruciate ligament in response to rotatory loads.,” J. Orthop. Res., **22**(1), pp. 85–89.
[44] Yagi, M., Wong, E. K., Kanamori, A., Debski, R. E., Fu, F. H., and Woo, S. L., 2002, “The American Journal of Sports Medicine Biomechanical Analysis of an Anatomic Anterior Cruciate Ligament Reconstruction,” pp. 660–666.
[45] Kanamori, A., Sakane, M., Zeminski, J., Rudy, T. W., and Woo, S. L.-Y., 2000, “In-situ force in the medial and lateral structures of intact and ACL-deficient knees,” J. Orthop. Sci., **5**(6), pp. 567–571.
[46] Pioletti, D. P., Rakotomanana, L. R., and Leyvraz, P. F., 1999, “Strain rate effect on the mechanical behavior of the anterior cruciate ligament-bone complex.,” Med. Eng. Phys., **21**(2), pp. 95–100.
[47] Nolan, D., Gower, A., Destrade, M., Ogden, R., and McGarry, J., 2014, “A robust anisotropic hyperelastic formulation for the modelling of soft tissue,” J. Med. Behav. Biomed. Mater., **39**, pp. 48–60.
[48] Bischoff, J., Siggelkow, E., and Sieber, D., 2008, “Advanced material modeling in a virtual biomechanical knee,” Abaqus Users Conf., pp. 1–15.